Molecular Vision 2026; 32:232-253 <http://www.molvis.org/molvis/v32/232>
Received 17 September 2025 | Accepted 9 February 2026 | Published 22 June 2026

Reporter-guided photoreceptor differentiation in 2D culture using PGP1-hIPSCs: A comparable alternative to 3D organoid systems?

Davinia Beaver,[1] Adrian C. Cioanca,[2] Nigel L. Barnett[1]

[1]Clem Jones Centre for Regenerative Medicine, Faculty of Health Science & Medicine, Bond University, QLD Australia; [2]Clear Vision Research Laboratory, The John Curtin School of Medical Research, College of Health and Medicine, The Australian National University, ACT, Australia

Purpose: To develop and characterize a xeno-free, two-dimensional (2D) differentiation protocol for directing human induced pluripotent stem cells (hIPSCs) toward photoreceptor (PhR)–like cells, using a live-reporter system and transcriptomic analysis to evaluate lineage fidelity and maturation compared to the three-dimensional (3D) culture paradigm.
Methods: A CRISPR/Cas9-engineered PGP1 hIPSC line expressing fluorescent reporters for retinal markers (*VSX2*, *BRN3B*, and *RCVRN*) was differentiated in adherent culture using chemically defined media supplemented with small molecules (T3, DAPT, taurine, and retinoic acid). Differentiation was assessed over time by immunocytochemistry, flow cytometry, reverse transcription quantitative polymerase chain reaction, ultrastructural imaging (transmission electron microscopy and scanning electron microscopy), and bulk RNA sequencing. Comparative transcriptomic analysis with 3D retinal organoid data was conducted to evaluate developmental kinetics and pathway enrichment.
Results: The 2D protocol reproducibly generated PhR-like cells expressing PhR-associated protein markers, including CRX, NR2F2, RCVRN, THRβ OPSIN-S, OPSN-M/L, and ARR3. Flow cytometric analysis demonstrated 93.6%, 96.2%, and 70.3% of RCVRN, OPSN-M/L, and OPSN-S positive populations at day (D) 42, while up to 97.4% of cells stained positive for RCVRN by D52. Early commitment to a PhR lineage was evident by D30, supported by transcriptional profiles consistent with PhR-like ontogeny. Ultrastructural analyses revealed features of putative inner and outer segments, including developing cilia and disc-like "whorls" supported by expression of gap junction protein markers and cilium markers (TMEM138 and CX36). Bulk RNA sequencing demonstrated faithful temporal regulation of PhR gene networks and highlighted accelerated differentiation compared to 3D cultures.
Conclusions: This pilot xeno-free 2D differentiation protocol offers a timely and scalable method for generating PhR-like cells from hIPSCs comparable to standard 3D culture systems. The results validate its downstream utility for retinal cell therapy development, high-throughput screening, and transplantation outputs pending further investigation, while supporting the transcriptome dominance model as a framework for evaluating photoreceptor fate acquisition in this culture paradigm.

Age-related macular degeneration (AMD) and retinitis pigmentosa (RP) are prevalent ocular pathologies classified as retinal degenerative diseases. These conditions affect a significant number of individuals worldwide, with approximately 200 million people living with AMD [1] and over 1.5 million affected by RP [2]. Most of these individuals will eventually experience partial or even complete loss of vision.

A shared characteristic among all retinal degenerative diseases is the damage inflicted upon the two types of light-sensing photoreceptor (PhR) cells, the rods and cones. These photon-capturing cells transform light signals into electrical impulses that are vital for vision production.

Correspondence to: Davinia Beaver, Bond University, Clem Jones Centre for Regenerative Medicine, Faculty of Health Science and Medicine, 14 University Drive Robina, Gold Coast, Queenland 4226, Australia; Phone: 0410183825; FAX: (07) 5595 1111; email: dbeaver@bond.edu.au

In AMD, the damage is greatest in the cone-dense region of the retina's macula. This region is responsible for acuity and central vision [3]. Progression of damage during retinal degenerative pathologies leads to irreversible destruction of these cells. There is no significant treatment to target these later stages of degeneration [4–6].

Pluripotent stem cell (PSC)–derived treatments are being considered as a possible therapeutic solution for retinal pathology to reverse the loss of vision by replacement of damaged PhRs with healthy new ones [7]. Earlier monolayer-based differentiation systems established important developmental principles for photoreceptor specification, particularly in murine models [8,9]. While these studies laid fundamental groundwork for in vitro retinal differentiation, clinical translation efforts in human systems have converged primarily on three-dimensional (3D) retinal organoid platforms and thus serve as the principal comparator in the present study.

Protocols to generate PhRs from human PSCs have primarily relied on 3D retinal organoid systems, which

model human retinal development with high fidelity [10–13]. However, these methods are primarily constrained by protracted culture durations, with limited scalability for downstream clinical translation [14].

The transcriptome dominance model provides a comprehensive framework for understanding how PhR cell types are specified and maintained through tightly regulated gene expression [15–18]. Central to this model are transcriptional hierarchies, where specific transcription factors act at various levels to activate or repress genes critical for PhR subtype differentiation. These transcription factors function within gene regulatory networks, coordinating the temporal and spatial activation of gene sets to ensure the orderly progression of PhR development. The model also incorporates feedback mechanisms, whereby gene products modulate transcription factor activity to fine-tune and stabilize cell identity. Epigenetic regulation, including DNA methylation and histone modifications, further reinforces gene expression patterns essential for long-term PhR maintenance. Importantly, the model accounts for the interplay of intrinsic factors and extrinsic cues, such as growth factors and cell–cell interactions, which together guide PhR specification. Although the transcriptome dominance model continues to evolve, the present study leverages its established principles to track and evaluate the molecular progression of a directed PhR differentiation protocol.

In this study, we report the development of a xeno-free, chemically defined two-dimensional (2D) differentiation protocol that guides human induced PSC (hIPSC)–derived cells through the progressive stages of PhR development using small molecules and cytokines that mimic key developmental cues. This adherent system offers a tractable and scalable alternative to 3D cultures, significantly reducing differentiation time and avoiding the need for any genetic enrichment strategies.

Retinal lineage progression was assessed using a triple transgenic reporter hIPSC line. Expression of *VSX2*-cerulean and *RCVRN*-mCherry, combined with immunocytochemistry, flow cytometry, and reverse transcription quantitative polymerase chain reaction (RT-qPCR), confirmed the emergence of substantial photoreceptor-like populations expressing cone-specific markers within the first 6 weeks of culture. Furthermore, using comparative transcriptome analysis with 3D retinal organoids, we demonstrate that this 2D system induces earlier expression of PhR-specific genes, consistent with a transcriptional dominance model of PhR development.

This pilot differentiation study was undertaken to evaluate the feasibility of the protocol and to observe early biological trends in PhR marker expression, rather than to generate statistically powered outcomes. The primary objective of this proof-of-concept investigation was to develop a clinically relevant strategy for generating PhR-like cells within an accelerated time frame, offering potential advantages for downstream applications such as suspension-based transplantation therapies. The findings demonstrate that the 2D differentiation protocol drives cells through a faithful, stepwise trajectory toward a PhR-like identity. This protocol could offer translational promise, positioning it as a viable alternative to the more complex and time-intensive organoid-based systems.

METHODS

Human induced pluripotent stem cells: The PGP1-hIPSC reporter line [19] was obtained from Robinson & Del-Tsonis (Miami University, Oxford, OH). This CRISPR/Cas9-engineered, triple transgenic line expresses fluorescent markers for early retinal cell types: *VSX2*-cerulean (neural progenitor), recoverin (*RCVRN*)–mCherry (pan-PhR), and *BRN3b*-GFP (retinal ganglion cell). This system enables real-time tracking of cell fate transitions from pluripotency through eyefield progenitor cells, neural retinal progenitor cells, and PhR commitment. Use of hIPSCs was approved by the Bond University Human Research Ethics Committee (BUHREC; protocol RO1740).

PGP1-hIPSCs at passage (p) 46 (experiment 1), p49 (experiment 2), and p60 (experiment 3) were cultured feeder-free on hESC-qualified Matrigel (BioStrategy, Macquarie Park, Australia) and maintained in mTeSR complete medium (StemCell Technologies, Rhodes, Australia) with daily media changes. Prior to differentiation, cells were transitioned to growth factor reduced Matrigel. Cells were seeded at ~150,000 cells/cm^2 and transitioned to primary differentiation medium (day [D] 1; Appendix 1) upon reaching ~90% confluence [20,21]. On D7, cells at ~70% to 80% confluence (~50,000 cells/cm^2) were passaged with Collagenase IV (ThermoFisher Scientific, Scoresby, VIC, Australia). Rock inhibitor (10 µM) (Focus Bioscience, Tingalpa, QLD, Australia) was added 1 h before each passage to enhance yield, minimize stress, and support survival [22].

Given the postmitotic nature of PhR cells, passage timing was guided by cell morphology assessment and proliferation rates. Gentle Cell Dissociation Reagent (StemCell Technologies) was used for enzyme-free dissociation. As single-cell passage proved ineffective, cultures were passaged as clumps, limiting accurate cell counting during secondary differentiation.

Murine 661W PhR cells as control: The immortalized murine PhR 661W cell line [23,24], provided by Dr. Muayyad

Al-Ubaidi (University of Oklahoma, Norman, OK) and obtained through Dr. Krisztina Valter-Kocsi (Australian National University, Canberra, Australia), was used as a control for immunocytochemistry (ICC), flow cytometry, and microscopy analysis. Cells were cultured in high-glucose Dulbecco's modified Eagle's medium with HEPES (ThermoFisher Scientific), 10% fetal bovine serum (Cytiva, Macquarie Park, NSW, Australia), 0.5% Glutamax (ThermoFisher Scientific), and 1 µl/ml 2-Mercaptoethanol (Merck, Bayswater, VIC, Australia).

Cells were maintained on uncoated Costar tissue culture (TC)-treated plates and passaged at ~80% confluency using TrypLE (ThermoFisher Scientific). Detached and resuspended cells were centrifuged at 300g for 3 min, reseeded, and cultured at 37 °C, 5% CO_2, and 90% relative humidity.

Differentiation medium and supplementation: From D0, primary differentiation medium guided the cultures toward the eyefield and neural retina, with medium changes every 2 to 3 days. On D8, secondary differentiation medium was introduced to enhance neural induction and PhR lineage commitment. Supplements included triiodothyronine (T3, D9; Sigma-Aldrich, St. Louis, MO), DAPT (D19; Sigma-Aldrich), taurine (D23; Sigma-Aldrich), and retinoic acid (D33; Sigma-Aldrich) and were maintained until D66 and D111. The complete list of reagents is detailed in Appendix 1 and Appendix 2.

Immunocytochemistry: Cells were fixed in 4% paraformaldehyde (PFA) for 10 min, permeabilized in blocking buffer (95% $DPBS^{-/-}$, 0.3% goat serum, 0.3% Triton X-100) for 1 h, and incubated overnight at 4 °C with primary antibodies, 1:100 prepared in Antibody Dilution Buffer (ADB: DPBS; Sigma-Aldrich, supplemented with 10% bovine serum albumin and 0.3% Triton-X). Antibodies are listed in Appendix 3. Secondary antibodies prepared in ADB (1:1,000; Appendix 4) were applied for 1 h at room temperature. Nuclei were stained with 20 µM Hoechst 34,580 for 10 to 15 min. Coverslips were mounted using Dako (Agilent Technologies, Mulgrave, VIC, Australia) Fluorescence Mounting Medium.

Confocal and live-cell microscopy: Following immunocytochemical staining of cultured cells, samples were imaged using an Olympus FV3000 confocal microscope (Evident, Macquarie Park, NSW, Australia) with Fluoview FVS315-SW analysis software (version 2.3.2.169 Evident), a Nikon Eclipse Ti-DH fluorescent microscope (Nikon, Rhodes, NSW, Australia), or a Live Cell Nikon Ti-E Inverted microscope (Nikon DMi1–468798) with NIS-Elements Advanced Research Software (version 5.02.03; Nikon). Live cells were monitored throughout the differentiation process and imaged using an Olympus DP23M digital microscope (Evident) with CellSens Standard software (version 4.2; Evident). Images of comparative samples were acquired under related settings within each experiment and exported as raw OIR (Olympus) or ND2 (Nikon) files, respectively, and converted to TIFF or JPEG files after analysis. Images of comparative samples were acquired under similar settings within each experiment and exported as raw OIR (Olympus) or ND2 (Nikon) files, respectively. Images were processed using ImageJ software (version 1.4f; National Institutes of Health, Bethesda, MD, USA). Individual color channels were first separated and saved, after which they were recombined to generate the final TIFF composite image.

Flow cytometry: Cells were dissociated with TrypLE and processed in FACS buffer ($DPBS^{-/-}$, 2% bovine serum albumin, 0.01% sodium azide). After permeabilization in blocking buffer (30–60 min, on ice), cells were stained with primary antibodies (1:100, 60–90 min) and secondary antibodies (1:1,000, 30 min; Appendix 2 and Appendix 3). For experiment 2, D52 cultures were stained for RCVRN; 661W cells served as positive controls. Negative controls were incubated with secondary antibody only (goat anti-mouse IgG [H^+L], Alexa Fluor 488; ThermoFisher Scientific). In experiment 3, D42 and D49 samples were stained for OPSIN-S, OPSIN-M/L, or RCVRN, with 661W and unstained samples as positive or negative controls, respectively. Data were acquired on a BD FACSAria Fusion and analyzed with FACSDiva v9.0 (Macquarie Park, NSW, Australia). Detailed flow cytometric gating strategies, including cell population selection, control samples, and marker-specific analyses, are shown in Appendix 5, Appendix 6 and Appendix 7.

RT-qPCR for the identification of development from hIPSC-PhR progenitors: RNA was extracted using the Quick-RNA Miniprep Kit (Zymo Research Integrated Sciences, Chatswood, NSW, Australia) per manufacturer instructions, with additional concentration and clean-up using RNA Clean & Concentrator-5 (Zymo Research) as needed. First-strand complementary DNA (cDNA) synthesis was performed using the iScript cDNA Synthesis Kit (Bio-Rad, Gladesville, NSW, Australia 1,708,890) with 200 ng input of RNA material.

RT-qPCR reactions were run using the SsoFast EvaGreen Supermix (Bio-Rad, 1,725,201) with 500 nM forward and reverse primers, at 95 °C for 30 s, 40 cycles of (1) denaturation at 95 °C for 5 s and (2) annealing and extension at 60 °C for 5 s with a final melt curve. Data analysis used Bio-Rad CFX Maestro v2.3 software, with fold changes calculated using the ΔΔCT method. GAPDH served as the reference gene [25], and fold change values were calculated based on maximum expression for each gene target. Gene targets were selected based on their role in the transition from pluripotency to PhR

progenitor fate, consistent with previous in vitro studies. Primer sequences were obtained as predesigned KiCqStart primers (Merck KSPQ12012 or Integrated DNA Technologies, Coralville, IA), detailed in Appendix 8 with results presented in Appendix 9.

Topological analysis:

Transmission electron microscopy—Cells were fixed in 4% PFA and 2.5% glutaraldehyde in 0.1 M sodium cacodylate buffer, postfixed in 1% osmium tetroxide, and dehydrated in graded ethanol. Samples were embedded in LX112 resin and polymerized at 60 °C overnight. Ultrathin sections (80 nm) were cut using a Leica Microsystems (Mt Waverley, VIC, Australia) UC6 ultramicrotome, stained with uranyl acetate and lead citrate, and imaged on a JEOL 1011 (Peabody, MA) transmission electron microscope at 80 kV.

Scanning electron microscopy: On D99 of experiment 3, cells were fixed in 3% glutaraldehyde, dehydrated in graded ethanol, rinsed with hexamethyldisilazane (Sigma-Aldrich), and air-dried overnight. Samples were mounted on stubs, gold-coated (JEOL Smart Coater), and imaged using a JCM-5000 NeoScope scanning electron microscope (Peabody, MA). Images were analyzed with NeoScope v1.2.3.

Summary of time course cell analysis: To monitor cell differentiation and development in culture, samples were taken at key developmental time points for analysis of marker expression using ICC, gene expression using RT-qPCR analysis, and subset marker analysis using flow cytometric analysis. Additionally, cells were pelleted and preserved for bulk RNA sequencing. For ICC, cells were collected at six time points (experiment 1: D0-IPSC, D6, D30, D46, D52, and D66). Cells were stained with specific antibodies followed by secondary fluoresceinated antibodies. Controls were exposed to secondary antibodies only. Control antibody staining is shown in Appendix 10. For gene expression analysis, cells were harvested at five time points (experiment 1: D0-IPSC, D6, D30, D40, and D59) for RT-qPCR analysis. *GAPDH* was used as a housekeeping reference gene [25]. Cells for bulk RNA sequencing were collected at five time points (experiment 1: D0-IPSC, D9, D30, D40, and D53).

To monitor cell differentiation and assess the reproducibility of the original protocol developed, samples were taken as close to the previous time points in differentiation as possible for ICC analysis, RT-qPCR, flow cytometric analysis, and collection and pelleting of cells for bulk RNA sequencing. For ICC, cells were collected at six time points for each subsequent experiment (experiment 2: D9, D31, D42, D52, D61, and D66; experiment 3: D9, D36, D43, D52, D66, and D111). For RT-qPCR, cells were harvested for analysis at five time points (experiment 2: D0-IPSC, D7, D30, D45, and D66; experiment 3: IPSC, D9, D30, D45, and D66). Flow cytometric analysis was performed at one time point, D52, for experiment 2 and two time points, D42 and D49, for experiment 3. Cells for bulk RNA sequencing were collected at five time points for experiment 2 (D0-IPSC, D9, D30, D45, and D66) and seven time points for experiment 3 (D0-IPSC, D7, D30, D45, D50, D66, and D111; time points analyzed and assays used are listed in Appendix 11, Appendix 12, and Appendix 13).

Transcriptome analysis: Raw sequencing reads for monolayer cultures were assessed for quality and adaptor or index contamination using FastQC, then aligned to the human reference genome (Hg38) using the Rsubread package with default parameters. Gene-level count matrices were generated by mapping aligned reads to the GENCODE comprehensive gene annotation (GRCh38.p14) using featureCounts. Count matrices for organoid cultures were downloaded from GSE119274. Raw counts were normalized using the trimmed mean of M-values method to account for library size differences. Genes with low expression, defined as fewer than 1 count per million in more than 70% of samples, were excluded from downstream analyses. Dimensionality reduction was first performed via principal component analysis (PCA) on gene-wise scaled expression values, followed by uniform manifold approximation and projection to facilitate visualization of global transcriptional patterns. Differential expression analysis was conducted using the limma–voom pipeline. Briefly, the voom function was used to estimate the mean–variance relationship of log-counts, which were then modeled using linear modeling (lmFit) and moderated with empirical Bayes (eBayes) shrinkage. Significantly differentially expressed genes were identified using topTable, adjusting for multiple testing. Gene set enrichment and pathway analyses were performed on differentially expressed gene lists to identify functional annotations and regulatory pathways.

RESULTS

PGP-1–reporter live fluorescence and morphological changes observed during differentiation: The PGP1-hIPSC line, engineered to express fluorescent reporters for retinal development markers, was used in this study. An experimental outline is illustrated in Figure 1A. This line, previously validated for differentiation into neural retina and PhR progenitors [26], enables real-time monitoring via live fluorescence, eliminating the need for cell sacrifice for endpoint assays. Daily culture assessments were conducted

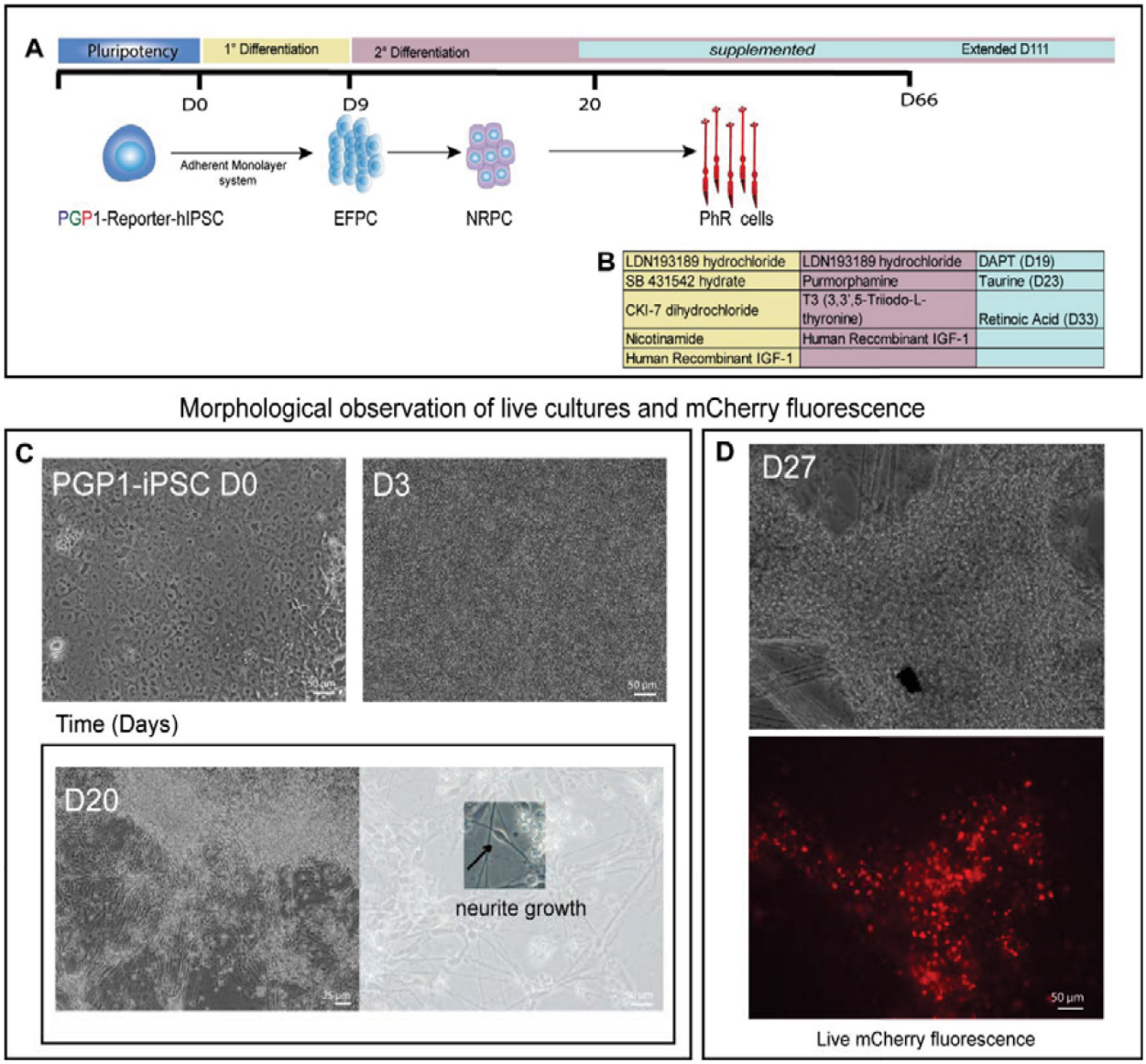

Figure 1. Pilot differentiation timeline and morphological progression of PGP1-hIPSCs toward photoreceptor lineage. **A**: Schematic of the pilot differentiation protocol. PGP1-hIPSCs were cultured in primary medium from Day 0 (D0) to D8 to induce eyefield progenitor cells (EFPCs), followed by neural induction medium from D9 to promote neural retina progenitor cells (NRPCs), with additional supplementation to guide photoreceptor (PhR) lineage specification. **B**: Overview of small molecules used during differentiation. Supplementation included T3 (D9), DAPT (D19), taurine (D23), and retinoic acid (D33). Full medium composition is provided in Appendix 1 and Appendix 2. **C**: Representative cell morphology from D0 (i.e., IPSCs) to D3 in primary medium compared to D20 in secondary medium, where neurite outgrowth is evident. **D**: Live fluorescence imaging at D27 revealed RCVRN-mCherry reporter expression, indicating photoreceptor lineage commitment.

by tracking cerulean (*VSX2*) and mCherry (*RCVRN*) signals; GFP (*BRN3B*) was not detected and is not discussed.

The earliest stages in driving progenitors toward a PhR commitment involve the inhibition of NOTCH signaling. Figure 1B summarizes the small molecules used in the primary and secondary medium. Here, DAPT (γ-secretase inhibitor) is used as a NOTCH inhibitor [27] and was added to the medium on D19 to drive PhR commitment. Similarly, taurine is a vital signaling molecule for PhR development [28] and is prevalent across the entire retina. Endogenous taurine is a cysteine derivative that has been shown to induce neural

development and maintenance and promote differentiation to PhR terminal fate [29,30]. Taurine deficiencies in rodents, cats, and primates reveal the inability of PhRs to mature [31]. T3, an activator of thyroid hormone receptors, was used from the onset of secondary differentiation (D9) as it is thought to influence and promote specifically cone fates [32]. When used in vivo and in vitro in organoid studies, T3 demonstrates a propensity to determine cone fates as well as diversity within cone subtypes [33]. Retinoic acid was added as a final supplement at later stages of secondary differentiation (D33). It regulates NRL expression and, therefore, rod fate [34]. Live morphological changes were observed throughout, with rosette formation and neurite outgrowth observed around D15 to D20 (Figure 1C). Cells were harvested upon fluorescence detection, with mCherry (*RCVRN*) expression first observed at D27 of the initial pilot experiment (Figure 1D).

Emergence of a PhR phenotype: Retinal progenitor cell development began with the emergence of eyefield markers characteristic of the anterior neural ectoderm, visualized via ICC (Figure 2A). At D6 of differentiation, cultures continued to express the pluripotency-associated markers, OCT4 and SOX2, as shown by nuclear localization in most cells. Concurrently, upregulation of early eyefield transcription factors RAX, PAX6, and LHX2 was observed, indicating the onset of retinal lineage specification in response to exogenous patterning cues present in the differentiation medium.

Following transfer to neural induction medium, cultures exhibited marked morphological changes, with sequential supplementation of T3 (D9), DAPT (D19), taurine (D23), and retinoic acid (D33). By D30, ICC revealed the presence of neural retina progenitor and proliferation marker CHX10 in the presence of NR2F2 (Figure 2A). By D46, coexpression of RCVRN and NR2F2 indicated the initiation of PhR lineage commitment, while CHX10 expression was notably reduced. RAX expression persisted alongside PRDM1, consistent with a transitional progenitor state and early PhR identity. By D66, cells exhibited markers of mature PhRs, including OPSIN-M/L and RCVRN, signifying further differentiation toward a committed PhR-like phenotype.

Gene expression changes from pluripotency to a PhR-like identity: Gene expression dynamics from pluripotency toward a PhR-like fate were assessed by RT-qPCR, normalized to *GAPDH* [25] and expressed as a percentage of each gene's maximum expression (Figure 2B). The RT-qPCR plot shows biological trends; accordingly, the results are descriptive trends only. *OCT4* declined steadily from D0, remaining low until a slight increase from D40. *OTX2* is involved in early ocular genesis and in subpopulations of progenitor cells that primarily produce cones [35]. Here we report a steady expression until D30, after which we observed an apparent increase. The neural retina progenitor marker *VSX2* increased to D6, followed by a transient decrease at D30, whereafter it resumed its increase. *PRDM1* was undetectable until D6, increased sharply to D30, then declined gradually after D40. The PhR commitment marker *CRX* was noticeably upregulated as early as D6 with peak expression seen at D30, followed by a transient decline by D40 with a subsequent increase toward the final time point. *NR2F2* and *RCVRN* followed similar trends, with low early expression and steady upregulation from D30 onward, indicating progression toward a PhR lineage. NR2F2 and RCVRN, both encoding PhR progenitor genes, showed an apparent increase in expression from D30.

Reproducible and efficient differentiation toward a PhR lineage: Reproducibility of PhR differentiation was confirmed in experiments 2 and 3 using stage-specific protein markers. From D9 of both experiments, as illustrated in the representative images in Figure 3A, SOX2, a key marker that supports retinal progenitor proliferation, was observed. Eyefield transcription markers PAX6, SIX3, CHX10, OTX2, LHX2, and RAX were also detected at this time point [36,37]. By D31 (experiment 2; Figure 3B), OTX2 expression was maintained, with expression of markers of committed PhRs, CRX. OPSN-S expression was not clearly visible. In contrast, NR2F2 was abundantly expressed. RHO expression was not evident, whereas RCVRN was readily detected, along with PRDM1 and the neural marker TUJ1. A similar pattern was observed in experiment 3 on D36 (Figure 3C), and OTX2 expression was once again maintained with the emergence of PhR commitment marker CRX. OPSN-S was clearer at this time point with RCVRN. NR2F2 was again expressed with RxRg appearance, which some studies have shown to be localized to cone PhRs [38]. Expression of PRDM1 and TUJ1 was also noted at this time point.

At D42 of experiment 2, expression of CRX OPSN-S, RCVRN, LHX2, OTX2, PRDM1, and TUJ1 was maintained (Figure 3D). By D43 of experiment 3, concurrent expression of RHO and OPSIN-M/L indicated the emergence of both rod and cone PhR lineages (Figure 3E). By D52 of experiment 2 (Figure 4A), expression of RCVRN and ARR3 was evident, while CRX was not. OPSN-S was present, and TUJ1 and LHX2 remained expressed. Ki67-positive nuclei within the differentiating cell population demonstrated ongoing proliferative activity. Colocalization with RCVRN was not observed, consistent with the distinct subcellular localization of these respective markers.

By D52 of experiment 3 (Figure 4B), cultures expressed THRβ, ARR3, and OPSN-M/L, while NRL and RCVRN were

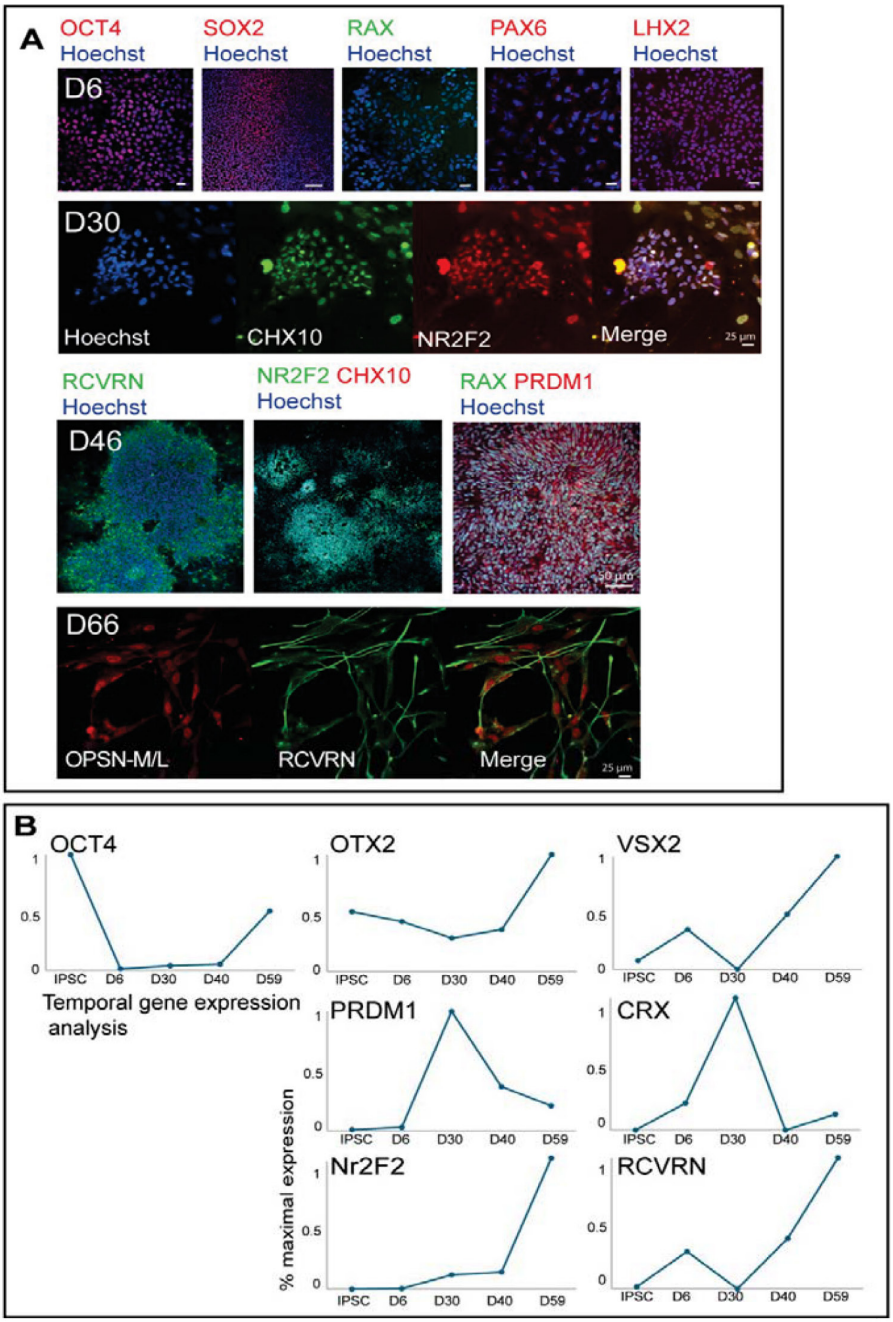

Figure 2. Stage-specific transcription factor and gene expression during retinal differentiation. **A**: Immunofluorescence analysis revealed dynamic expression of transcription factors and retinal markers across differentiation stages. At D6, pluripotency markers OCT4 and SOX2 were detected. During primary differentiation, the retinal neurogenesis markers RAX, PAX6, and LHX2 emerged. By D30, expression of the neural retinal progenitor cell (NRPC) marker CHX10 and photoreceptor (PhR) subtype-specifying marker NR2F2 was observed. At D46, RCVRN and NR2F2 were present alongside diminishing CHX10, with sustained expression of RAX and PRDM1. By D66, OPSN-M/L and RCVRN were detected. Cell nuclei were counterstained with Hoechst 33,342. **B**: RT-qPCR analysis of gene expression across five time points (D0, D6, D30, D40, and D59) during the differentiation protocol. Expression levels were normalized to GAPDH and presented as percentage of maximal expression for each gene. The data show expression then downregulation of pluripotency gene OCT4, followed by upregulation of eyefield gene OTX2, NRPC gene VSX2, and early PhR lineage markers PRDM1, CRX, RCVRN, and NR2F2.

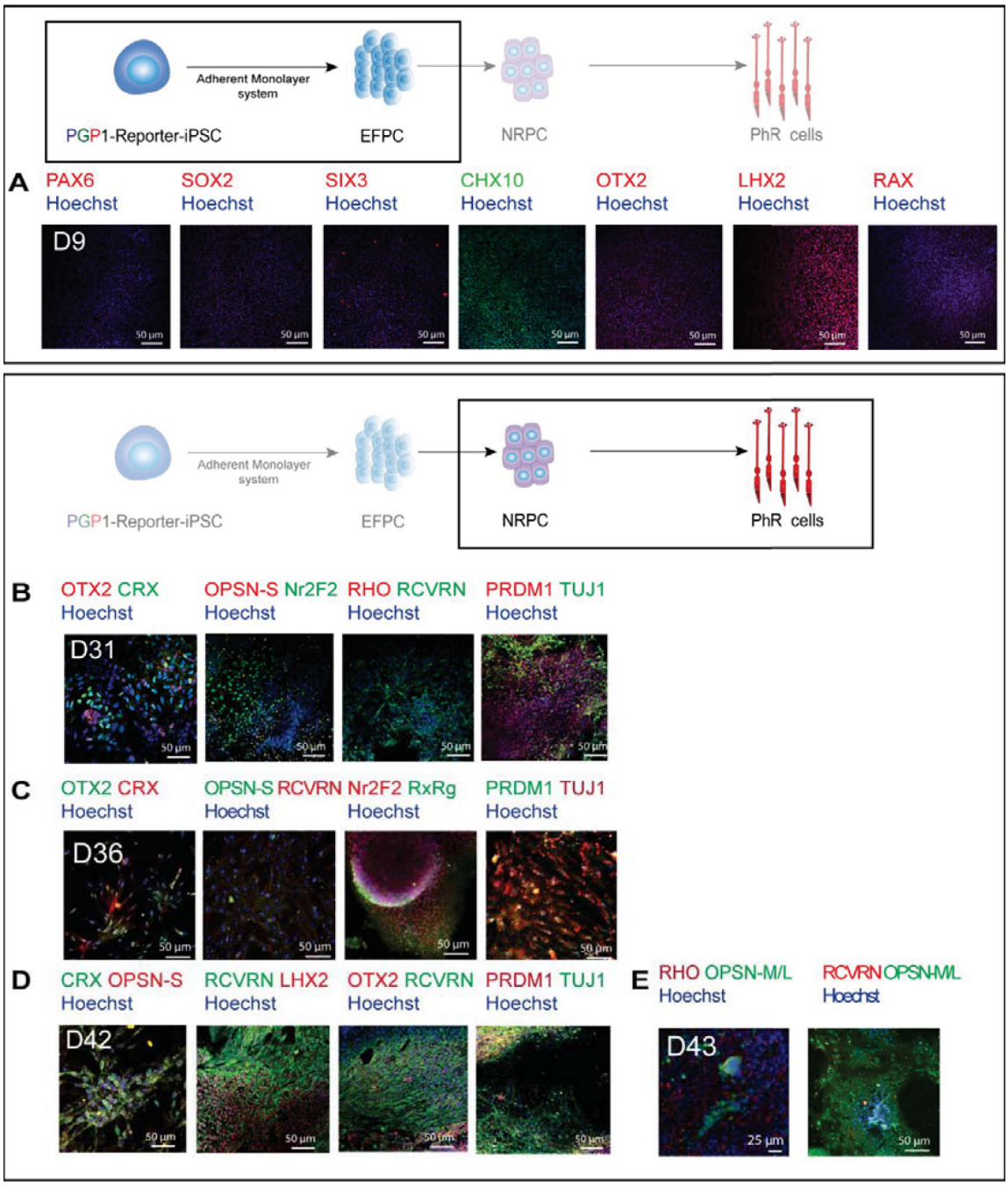

Figure 3. Temporal expression of retinal markers during differentiation (Days 9–43). **A**: Representative images from Experiments 2 and 3 showing expression of eyefield progenitor markers PAX6, SOX2, SIX3, CHX10, OTX2, LHX2 and RAX on D9. **B**: Immunofluorescence at D31 showed expression of OTX2 and CRX, with no detectable signal for OPSN-S or RHO. Expression of NR2F2, RCVRN, PRDM1, and TUJ1 was observed. **C**: At D36, expression of OTX2, CRX, OPSN-S, RCVRN, NR2F2, RxRg, PRDM1, and TUJ1 was evident. **D**: By D42, expression of CRX, OPSN-S, and RCVRN was maintained, along with LHX2. Some OTX2 expression persisted, and PRDM1 and TUJ1 remained detectable. **E**: At D43, immunocytochemistry revealed expression of RHO, OPSN-M/L, and RCVRN. Cell nuclei were counterstained with Hoechst 33342.

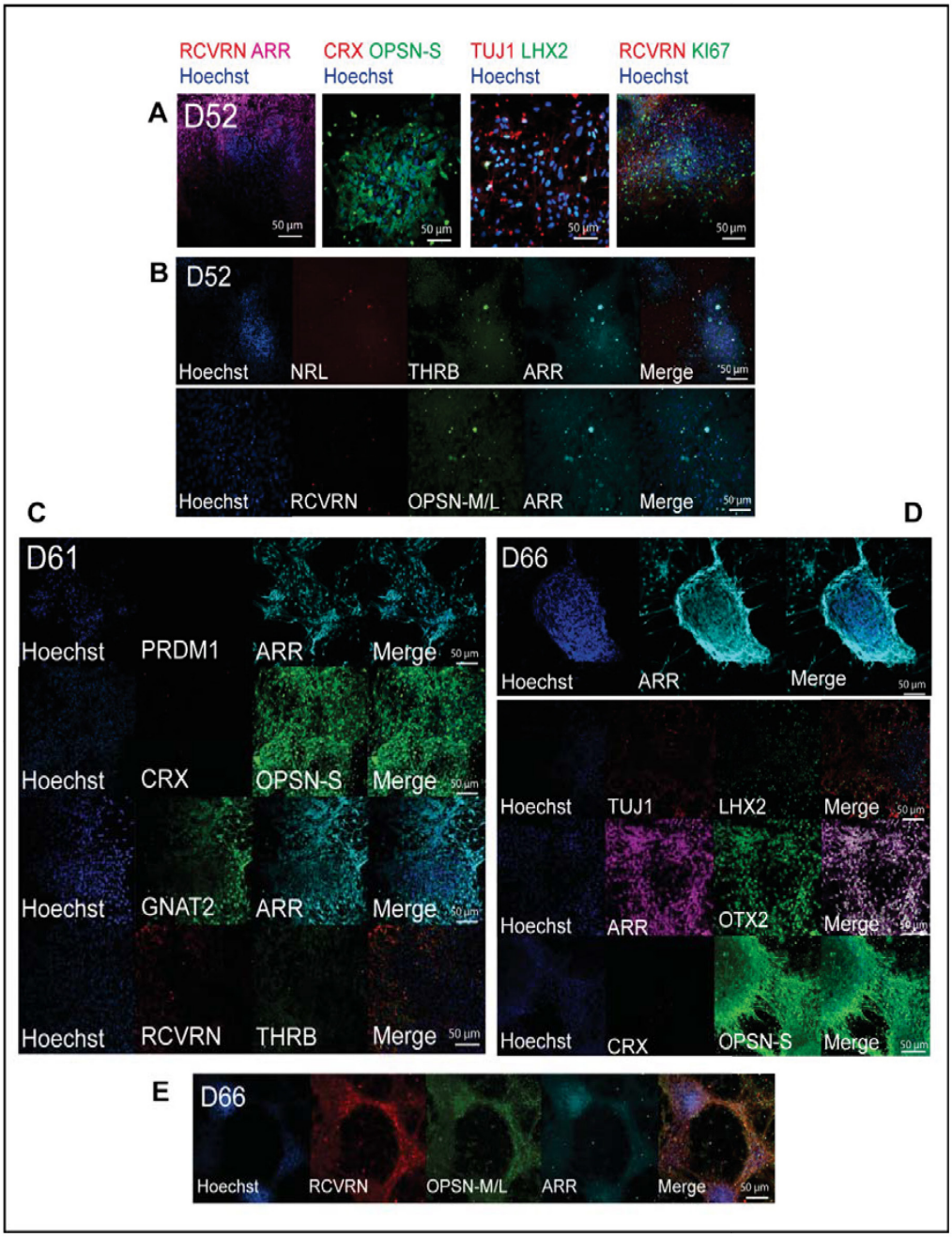

Figure 4. Representative immunofluorescence images from two independent experiments showing retinal marker expression during late differentiation (Days 52–66). **A**: At D52, cells expressed RCVRN, ARR3, CRX, OPSN-S, TUJ1, LHX2, and the proliferation marker K_i-67. **B**: At the same time point, NRL and RCVRN were absent, while THRβ, ARR3, OPSN-M/L were apparent. **C**: By D61, PRDM1 and CRX apeared absent, whereas ARR3, OPSN-S, GNAT2, RCVRN, and THRβ remained expressed. **D**: At D66, TUJ1 and LHX2 expression declined consistently across replicates, while RCVRN, OPSN-M/L, ARR3, OTX2, and OPSN-S were detected; CRX was barely detectable. Cell nuclei were counterstained with Hoechst 33,342. Circular or clustered staining patterns reflect regions of natural cell aggregation that occur at later differentiation stages due to preferential cell-cell association within the culture.

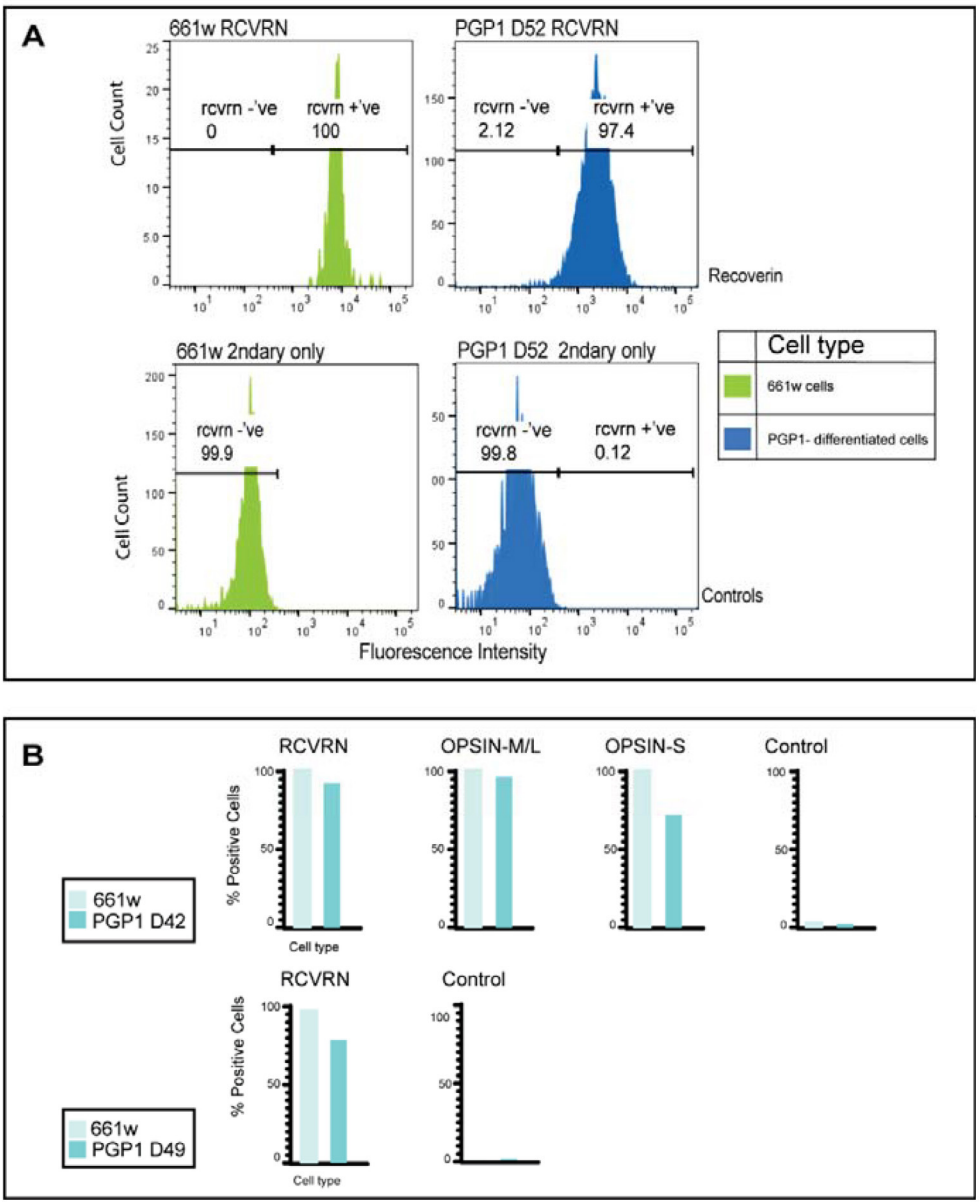

Figure 5. Flow cytometric analysis of retinal marker expression during differentiation. **A.** Flow cytometry of cells harvested from Experiment 2 at D52 showed 97.4% RCVRN-mCherry–positive cells, comparable to 99.9% positivity in 661W control cells. **B**. Analysis for Experiment 3 at D42 revealed 93.6% RCVRN, 96.2% OPSN-M/L, and 70.3% OPSN-S expression, relative to 661W positive controls. At D49, 93.3% of the population was RCVRN-positive, compared to 99.3% in 661W cells.

not detected. At D61 in experiment 2 (Figure 4C), staining for PRDM1, CRX, and RCVRN was reduced at this time point, whereas cone-specific markers ARR3, OPSN-S, GNAT2, and THRβ were more prominent. At the final time point, D66 of experiment 2 (Figure 4D), ARR3, OTX2, and OPSN-S expression persisted alongside diminishing TUJ1 and LHX2. Detected CRX levels varied between experiments. By D66 of experiment 3 (Figure 4D), all three PhR markers, RCVRN, OPSIN-M/L, and ARR3, were clearly expressed. The culture duration for experiment 3 was extended to D111, revealing sustained expression of both rod and cone PhR markers, RHO and OPSIN-S, via immunocytochemistry. Additionally, expression of the gap junction protein CX36 and the connecting cilium marker TMEM138 was observed. These findings, integrated with gene expression and ultrastructural data are discussed collectively in the Results section.

Flow cytometric detection of RCVRN and mature PhR marker expression: Live mCherry fluorescence, indicative of RCVRN expression, was detected as early as D24 in experiment 2 and D21 in experiment 3 (Appendix 14). By D52 of differentiation, 97.4% of cells in experiment 2 were RCVRN-positive by flow cytometry, compared to 100% in the 661W control population (Figure 5A).

Immunocytochemical staining revealed consistent expression of RCVRN, OPSN-S, and OPSN-M/L as early as D31 in experiment 2 and D36 in experiment 3 (Figure 3B,C). To quantify expression, flow cytometry was performed on cells collected at days 42 and 49 of experiment 3. At D42 (Figure 5B), 92.6% of cells were RCVRN-positive, 96.2% expressed OPSIN-M/L, and 70.3% expressed OPSIN-S. The 661W cells showed 99.9% positivity for all markers. By D49, 93.3% of cells were RCVRN-positive, compared to 99.3% in the 661W control. These markers were selected as they have previously been validated in the 661W cell line corresponding to PhR-like cell lineage [39–41].

Integrated morphological and transcriptomic analysis of PhR differentiation: PCA in Figure 6A illustrates dynamic changes in gene expression as cells transition from hIPSCs to PhR-like cells. Clustering of technical replicates confirms reproducibility and consistency within individual experiments (Figure 6B). Transcriptomic differences were observed across experimental groups. Experiment 1 showed greater variability in gene expression trends, while experiments 2 and 3 exhibited tighter clustering along the differentiation trajectory. Temporal gene expression patterns revealed pronounced shifts between hIPSC and early differentiation stages (D7–D9), particularly in experiments 1 and 2, followed by relative stabilization at later time points (Figure 6C).

Transcriptomic identification of photoreceptor pathways and morphological correlates: Heatmap visualization in Figure 6D illustrates dynamic gene expression patterns associated with PhR development across differentiation stages. Gene Ontology biological process enrichment analysis identified key pathways and genes associated with PhR development and maturation. Early time points showed expression of retinal progenitor genes, including *OTX2*, *PAX6*, *RAX*, and *LHX2*. By approximately D30, expression shifted toward committed PhR markers such as *RCVRN*, *CRX*, *THRβ*, *OPSN-S*, and *RORB*. Additional PhR-specific genes not previously examined (i.e., *ARMC9*, *EYS*, *MAP2*, and *IMPG2*) were also detected, supporting their involvement in PhR development. These data highlight the temporal activation and suppression of key regulatory genes, which likely correlate with distinct phases of PhR maturation. These transcriptomic findings informed subsequent morphological and ultrastructural analyses.

Scanning electron microscopy of PhR-like cells: Scanning electron microscopy (SEM) analysis of D99 cultures from experiment 3 (Figure 6E) revealed distinct morphological features consistent with PhR-like cells. The cells exhibited well-defined cell bodies (cb) and extended processes resembling connecting cilium (ml) observed in their neurite-like structure. Surface textures ranged from smooth to granular, suggesting different stages of differentiation or structural specialization. Cells appeared organized in clusters and interconnected networks, potentially reflecting in vivo–like maturation and increased cell-to-cell interactions. Some images showed connecting processes (potential plasma membrane projections [pp]) between cells, indicative of early structural communication or support mechanisms.

Transcriptomic and ultrastructural evidence of PhR maturation: Genes associated with PhR connecting cilium were upregulated during differentiation, suggesting tightly regulated timing for cilium assembly and function (Figure 7B). Transcriptomic analysis identified clusters of genes linked to outer segment development, indicative of advancing PhR maturation (Figure 7C). Although these genes were not the primary focus of earlier datasets, their expression patterns align with ultrastructural features observed via transmission electron microscopy (TEM; Figure 7A, D). The combined detection of connecting cilium and outer segment–related transcripts, along with immunocytochemical evidence of protein localization (Figure 7E), supports the emergence of putative outer segment structures at later time points. These findings provide molecular and morphological evidence for the maturation of PhR-like cells.

Ultrastructural analysis of differentiated PhR-like cells: TEM of hIPSC-derived PhR-like cells at days 50 and 64, alongside 661W controls (Appendix 15), revealed multiple ultrastructural features consistent with PhR-like morphology. At D50 (Figure 7A, B), cells demonstrated linear organization with identifiable inner segment–like and outer segment–like regions, calyceal process-like structures (cp), and abundant mitochondria (m). Vesicular structures were observed in proximity to the Golgi apparatus and within the cytoplasm. Whorl-like membranous structures were also present at later time points, particularly evident at D106 (Figure 7D).

Appendix 15 shows a cross section of D50 cells from experiment 3 arranged in a semi-organized layer with clearly identifiable nuclei (Nu) and prominent nucleoli. Cytoplasmic compartments containing mitochondria and Golgi apparatus were readily observed, together with membrane-bound vesicles and polarized cell morphology.

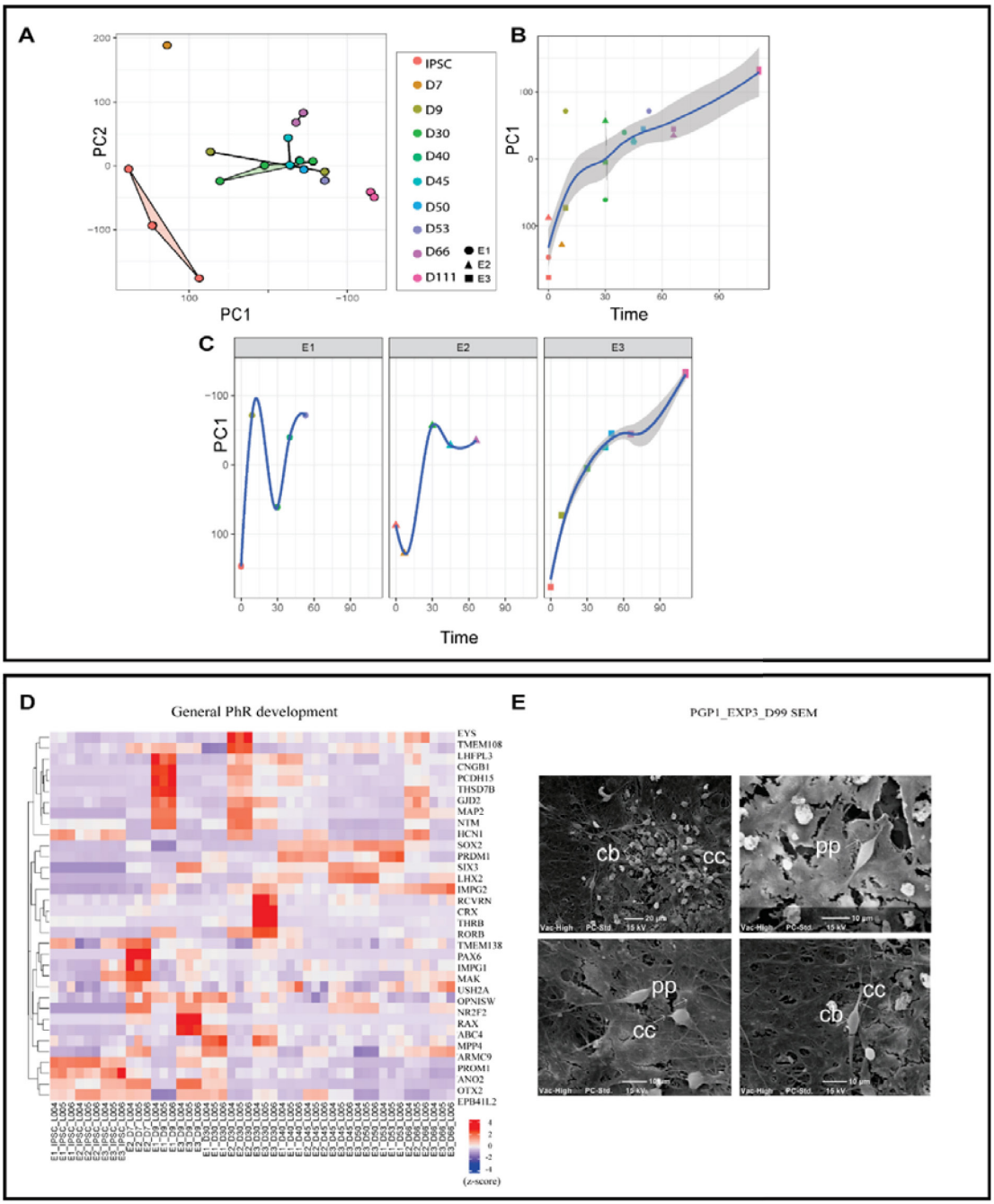

Figure 6. Principal component analysis (PCA) and characterization of hIPSC-derived photoreceptor (PhR) differentiation across three independent experiments. **A**: PCA plot showing technical replicates clustering closely, indicating reproducibility, while experimental groups display variation in gene expression across differentiation time points (D7, D9, D30, D40, D45, D50, D53, D66, D111). **B**: Combined PCA trajectory illustrating changes in the first principal component (PC1) over time across all experiments. **C**: Individual PCA trajectories of PC1 for each differentiation experiment (Exp 1, Exp 2, Exp 3), demonstrating a general upward trend in PC1 values over time, with variability during early differentiation stages. **D**: Heatmap of cluster analysis of differentially expressed genes, highlighting gene expression patterns associated with photoreceptor development across all three experiments and time points. **E**: Scanning electron microscopy of D99 differentiated cells (Exp 3), revealing surface morphology and spatial organization, including defined cell bodies (cb), presumptive connecting cilia (ml), and potential plasma membrane proteins (pp) suggesting intercellular connectivity.

Additional TEM imaging (Appendix 15) confirmed similar ultrastructural features in D50 cultures, including well-defined nuclei, cytoplasmic organelles, Golgi complexes, mitochondria, calyceal process–like structures, and putative inner segment regions. Fine membrane extensions resembling early neurite projections were also present between adjacent cells.

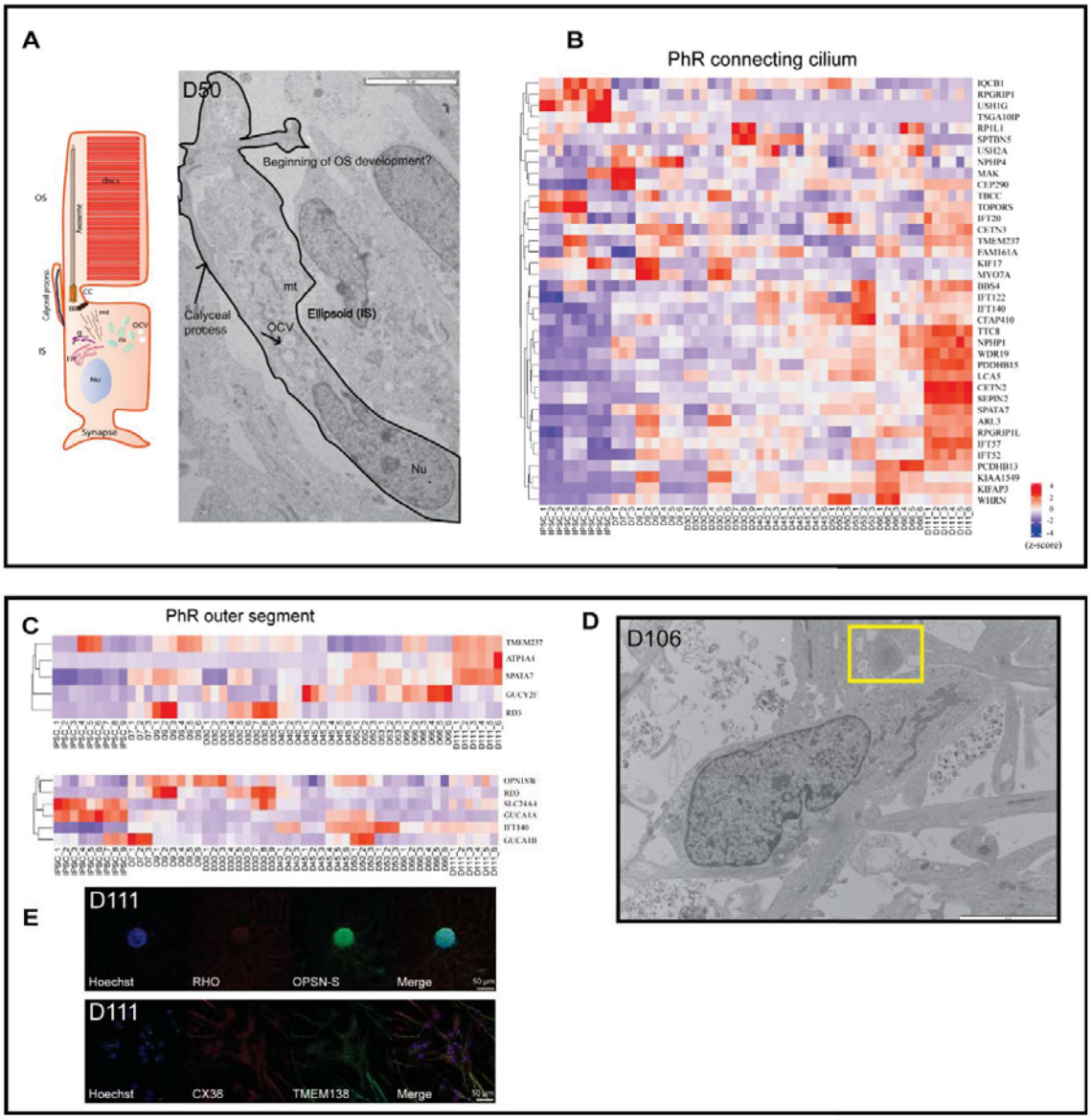

Figure 7. Ultrastructural and molecular characterization of hIPSC-derived photoreceptor-like cells. **A**: Schematic representation of a photoreceptor (PhR) cell highlighting key subcellular structures: discs, synapses, nuclei (Nu), endoplasmic reticulum (ER), mitochondria (m), Golgi apparatus (g), opsin-carrying vesicles (OCV), calyceal processes, outer segment (OS), inner segment (IS), connecting cilia (CC), and microtubules (mt). Transmission electron microscopy (TEM) of hIPSC-derived PhR-like cells at day 50 of differentiation (D50, Exp 3) reveals nuclei (Nu), IS, OS, calyceal processes (arrow), mitochondria (m), and putative OCVs. Scale bar: 10 µm. **B**: Heat map showing expression of genes associated with the connecting cilium across three differentiation experiments. Data are presented as gene-wise scaled z-scores. **C**: Heat map showing expression of genes associated with photoreceptor outer segments across three differentiation experiments. Data are presented as gene-wise scaled z-scores. **D**: TEM image of hIPSC-derived PhR-like cells at day 106 of differentiation (D106, Exp 3) showing abnormal organization of putative outer segments, appearing as 'whorls' (highlighted in yellow box). Scale bar: 5 µm. **E**: Immunofluorescence analysis of RHO, OPSN-S, CX36, and TMEM138 expression at day 111 of differentiation (D111). Nuclei were counterstained with Hoechst 33342.

Comparative TEM analysis of D64 experiment 3–derived PhR-like cells and immortalized 661W cells (Appendix 15) revealed notable morphological differences. In both cell types, nuclei were clearly identifiable, but 661W cells exhibited more uniform nuclear morphology and denser cytoplasmic organization. Mitochondria appeared more numerous and densely packed in 661W cells, whereas stem cell–derived PhR-like cells displayed a looser cytoplasmic arrangement with a more dispersed organelle distribution. These observations suggest that, while PhR-associated ultrastructural features are present in differentiated cultures, the overall cellular architecture differs from that of the immortalized 661W cell line.

At later differentiation stages (D106), TEM imaging revealed prominent whorl-like membranous structures consistent with ongoing putative outer segment–like membrane organization (Figure 7D). Integration of TEM and SEM datasets provides a framework for tracking morphological progression of hIPSC-derived PhR-like cells across differentiation time points.

Early transient photoreceptor commitment in 2D culture compared to organoid-based differentiation: A comparative analysis of selected genes was used to compare this culture paradigm to the more widely used organoid method of culturing in vitro retinal cells. Figure 8A demonstrates a diverging pattern across PC1. The monolayer method approximates a linear trajectory while the organoid cultures follow a more irregular average gene expression trend. Figure 8B presents a comparative analysis of gene expression profiles over time for selected transcription factors and markers associated with PhR differentiation, using this developed protocol and the more traditional organoid culture system. Organoid comparison data were obtained from [42]. The figure displays the temporal dynamics of multiple genes, including *CRX*, *LHX2*, and *NR2F2*, throughout the differentiation process, providing insights into the developmental trajectory under each culture condition.

The results highlight the temporal changes in gene expression across the differentiation process, with each subplot illustrating the distinct activation patterns of individual genes. These temporal patterns suggest different roles and activation timings during PhR differentiation, reflecting the complex regulatory processes involved. Both culture methods exhibit similar overall expression trends for most genes, indicating that both protocols can effectively induce PhR differentiation. However, differences in timing and amplitude of expression reveal important distinctions between the two approaches.

For genes such as *CRX* and *RAX*, the monolayer culture reaches peak expression earlier than the organoid culture, suggesting a faster commitment in the monolayer condition to a PhR final fate. Conversely, genes like *SIX3* and *PRDM1* show more sustained expression in organoid cultures, indicating prolonged activation and potentially a more gradual or complete differentiation pathway. This prolonged expression pattern in organoids could be attributed to the 3D structure, which provides a more in vivo–like environment, supporting better cell–cell interactions and niche signaling. The shaded areas surrounding the expression curves represent statistical variance in expression levels. Broader variance in some plots, such as *TMEM138* and *RCVRN*, might reflect higher heterogeneity in gene expression among replicates or cell populations within the culture system. Such variability could be due to differences in differentiation efficiency or the intrinsic heterogeneity of the cells being cultured. Gene-specific differences are particularly notable in this comparative analysis. Genes such as *NR2F2* and *RXRG* show distinct profiles between the two culture methods, with organoid cultures maintaining higher overall expression levels. This suggests that these genes might be more influenced by the 3D environment. Conversely, genes such as *SIX3* and *SOX2* exhibit highly synchronized patterns across both methods, implying that these genes are robustly regulated during differentiation, regardless of the culture system. The findings from this analysis indicate that while monolayer and organoid cultures follow divergent temporal differentiation kinetics, they ultimately converge on similar transcriptional programs, leading to a PhR fate.

DISCUSSION

These works have explored the development, characterization, and transcriptomic profiling of a novel protocol for differentiating hIPSCs into PhR-like cells. The research was motivated by the potential application of PhR cells in regenerative medicine, particularly for retinal diseases that cause irreversible loss of vision, such as AMD and RP. We present a comprehensive analysis, from the initial protocol development to in-depth characterization and gene expression profiling, highlighting the viability and potential of this differentiation protocol.

Initial exploration focused on developing a robust differentiation protocol. Traditional methods for PhR differentiation use more common 3D culture systems, often encountering limitations with long culture duration and challenges in enriching specific PhR subtypes [14]. To address these issues, a 2D monolayer culture approach was employed, incorporating a combination of small molecules to drive hIPSCs

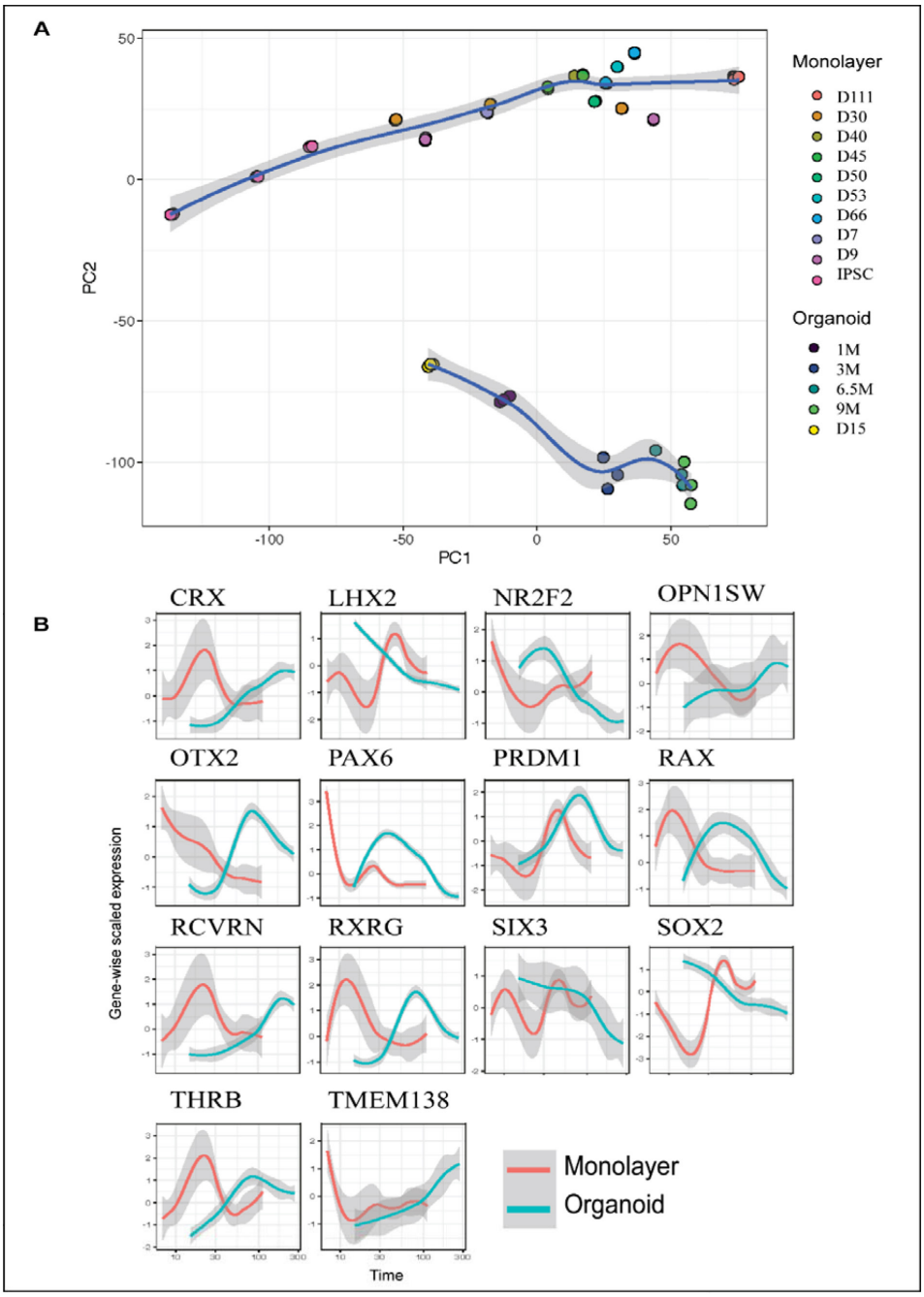

Figure 8. Comparative transcriptomic analysis of photoreceptor differentiation in 2D monolayer versus 3D organoid cultures. **A**: Principal component analysis (PCA) of average gene expression trajectories across all time points from three independent PGP1-IPSC photoreceptor differentiation experiments (top line) and retinal organoid differentiation obtained from [42] over a 9-month culture period (bottom line). The divergence in trend lines highlights substantial differences in transcriptional dynamics between the two culture paradigms. **B**: Expression profiles of a selected subset of genes monitored throughout differentiation, illustrating distinct expression patterns between monolayer directed differentiation and 3D organoid culture conditions.

through distinct developmental stages. The protocol aimed to generate a population of committed PhR progenitors capable of further maturation.

Key findings include the stepwise induction from eyefield progenitors to neural retina and progressively mature photoreceptors, validated by developmental markers aligned with the transcriptional framework of PhR development [18,43,44]. The sequential addition of supplements such as T3, taurine, DAPT, retinoic acid, and IGF-1 facilitated the progression through these stages, as evidenced by marker expression profiles captured using various analysis methods. Markers of stage-specific development during differentiation, from pluripotency to early PhR commitment, corresponded well with in vivo developmental transcriptome markers, confirming the capacity of the protocol to replicate essential stages of PhR development.

Limitations were observed with the use of the genetically modified PGP1-reporter line. Live fluorescence was detectable only when cells formed aggregates, making fluorescence detection in single cells challenging, particularly during dissociation for flow cytometric analysis. This challenge necessitated the harvesting of additional cells, and methods were then optimized to facilitate fixed, stained cultures to obtain quantitative analysis.

Double labeling with more representative markers of PhR cells and their progenitors may provide a more robust solution. Expanding the characterization of this protocol using a *CRX* reporter line [45] will enable more precise monitoring of PhR lineage commitment and facilitate real-time tracking of differentiation efficiency. As *CRX* is a required transcription factor for PhR development and specifies their postmitotic lineage, implementing the use of reporter lines like this will providing more specific and reliable labeling. However, CRX expression is variable and fluctuates with developmental age and light exposure [46], which may limit its reliability as a sole marker of PhR identity. At present, the most definitive markers for identifying committed PhR-like cells remain unclear, particularly given the dynamic expression patterns observed across development and differentiation platforms. In this context, double or multiplex labeling (e.g., antibodies, RNA probes, and reporter genes) may provide a more robust indication of PhR commitment and phenotype than any single marker alone. These findings underscore the need to apply a broader panel of molecular markers to improve in vitro characterization and posttransplantation tracking. They also highlight the importance of further elucidating the transcriptional networks that govern PhR lineage specification and maturation.

The reproducibility of the developed protocol was evaluated, where two additional independent experiments were conducted using the same differentiation methodology. Results demonstrated consistent expression patterns of PhR markers at multiple points across the differentiation timeline and through quantifying expression of some of the more commonly used markers listed in these works and guided by the literature. This reproducibility indicates that the underlying differentiation framework could inform future development of 3D culture systems; however, successful translation would require protocol redesign, including adjustments to patterning cues, culture architecture, and temporal signaling, rather than direct transfer of current conditions. With appropriate redevelopment, a 3D adaptation may enable the emergence of additional retinal cell types and more complex cell–cell interactions, producing tissue constructs that better recapitulate aspects of the in vivo retinal environment. Such systems would be more suitable for downstream applications such as disease modeling and drug testing, which depend on multicellular organization and signaling not achievable in the present 2D platform. Such enhanced cell–cell communication could generate tissues that more faithfully recapitulate the in vivo retinal environment, making the system more suitable for disease and drug testing. Future investigations may provide definitive confirmation.

The unexpected observation of RHO expression at D42 without corresponding NRL expression at D52 warrants further investigation into the controlled nature of retinal subpopulations during PhR development. This discrepancy may reflect transient ectopic expression, potentially representing a temporal snapshot of differentiation influenced by uncharacterized variables within the culture conditions. During PhR differentiation, Nr2E3 plays a pivotal role in activating transcription factors such as CRX and NRL. The latter, NRL, is assumed to repress cone fate and promote rod fate [47]. However, the developmental pathway is complex, and some cone precursors expressing OPSN-S may inadvertently contribute to rod populations, although the majority differentiate into S or M cones. It is important to note that commitment to either a rod or cone fate may not be mutually exclusive. Some subpopulations of cones could transiently express both rod-specific and cone-specific genes [48], thus providing an explanation for heterogeneity in the presented data. This suggests that the process of PhR fate determination involves a more nuanced interplay of regulatory factors, with potential overlap between rod and cone gene expression during early differentiation stages, a phenomenon that warrants further investigation.

OTX2 operates upstream of PRDM1/BLIMP1 [49]. PRDM1 and VSX2 engage in a mutually inhibitory relationship where PRDM1 suppresses VSX2 by binding to its enhancer region [50,51]. PRDM1-positive cells that express OTX2 are those that have committed to a PhR fate [52]. The relationship between VSX2 and PRDM1 is crucial for committing cells to their respective lineages. Upregulation of VSX2 promotes bipolar cell fate at the expense of PhRs and vice versa. *VSX2* mutants show nonfunctional messenger RNA in developing PhRs, indicating that OTX2-positive cells destined to become bipolar cells may have their fate suppressed by an overarching PhR program [52]. These presented data also capture this relationship between VSX2 and PRDM1.

The reproducibility of this protocol has led to the characterization of hIPSC-derived xeno-free PhRs without the use of any adeno-associated virus for labeling. Moreover, this culture paradigm yields large populations expressing mature PhR markers, including cone subtypes, at levels that are comparable to those reported in previous studies [7,44,53].

These repeated experiments aimed to quantify subpopulations that express committed PhR markers, and the data provide time points suggestive of large populations of medium- and long-wavelength cones by D42. It is evident from the data that PhRs have committed to their lineage by D30, while live fluorescence imaging suggests that recoverin expression begins almost 10 days prior.

The high degree of apparent coexpression between OPSN-S and OPSN-M/L observed in our cultures contrasts with the segregation seen in the mature human retina but is consistent with cone development in vivo. Studies from the Hendrickson laboratory have demonstrated that human fetal cones frequently exhibit dual S- and L/M-opsin expression during mid-gestation, representing a transient developmental state before terminal subtype specification [54]. These dual-labeled cones were reported throughout fetal stages and progressively decline with maturation, becoming rare only in the postnatal retina. Our findings therefore likely reflect an immature or transitional cone phenotype within the 2D differentiation environment, indicative of incomplete opsin regulatory refinement at the analyzed time points rather than aberrant fate specification.

An additional limitation of this study was the lack of thorough characterization of cell development between D9 and D15. These findings suggest that this time point represents the optimal window for the generation of PhR progenitors using this protocol. Further analysis across adjacent time points is expected to provide additional insights into the dynamics of PhR differentiation. Commitment to PhR lineage at these early time points was not expected initially, and so further development of the protocol will focus on this early developmental window.

Extending the differentiation period from D66 to D112, aligning with the culture durations commonly employed in 3D organoid protocols [55–57], revealed additional maturation features, particularly in the ultrastructural morphology of the differentiated cells. The appearance of putative outer segments demonstrated that cells produced may be capable of developing mature functional structures by the appearance of whorls. However, this result also indicates that specific signals are lacking to give accurate and complete development of PhRs. Despite this, discovery of these features demonstrates that cells undergoing differentiation are attempting to produce features that could define their functional phenotype. The electron microscope (EM) features observed in differentiated cultures seem consistent with early stages of PhR morphological maturation. The presence of polarized inner segment–like regions, calyceal processes, mitochondria enrichment, Golgi-associated vesicles, and whorl-like membrane structures suggests progression toward outer segment formation; however, these findings remain descriptive indicators rather than functional confirmation of mature photoreceptor activity. Definitive determination of active protein trafficking, vesicular opsin transport, and functional outer segment biogenesis will require future targeted approaches, including immunoelectron microscopy, molecular colocalization studies, and electrophysiological assessment. Comparison to the more organized ultrastructure of the 661W PhR cell line further indicates that while hIPSC-derived cells demonstrate some morphological patterning, full structural maturation likely remains incomplete at the analyzed time points. These EM observations represent hypothesis-generating morphological correlates rather than definitive evidence of complete outer segment development. Resolving these structures unequivocally will require future studies employing immuno-EM or serial block-face EM.

Transcriptomic analysis corroborated previous findings, demonstrating a well-coordinated transition of cells from an undifferentiated state to a PhR-type lineage, closely mimicking the developmental trajectory observed in vivo. When compared to established retinal organoid systems, the 2D monolayer system faithfully recapitulated key aspects of PhR development, with earlier expression of committed lineage markers, and offered advantages in both efficacy and ease of manipulation. While these results align with expectations and the broader goal of achieving higher yields with reduced handling and shorter differentiation times, certain limitations remain. Organoids continue to more accurately

replicate native retinal cell types due to their capacity to support complex cell-to-cell interactions. For clinical applications and transplantation, it is hypothesized that younger progenitor cells may offer a more viable therapeutic option. This underscores the importance of rapid and near-homogeneous generation of these cell types, a capability that this protocol may provide, pending further validation through long-term transplantation studies. The development of a reliable and reproducible differentiation protocol for generating PhR-like cells from hIPSCs has significant implications for both basic research and therapeutic applications. The protocol can serve as a platform for studying the molecular mechanisms underlying PhR development and disease, providing insights into the etiology of retinal degenerative diseases. On a transcriptomic level, further studies will provide a deeper understanding of the fate choice and subfate choices between PhR cells and what drives them. Single-cell RNA sequencing, histone methylation, and chromatin remodeling will be considered to understand the mechanisms governing cellular heterogeneity in differentiated cultures, thereby producing a more detailed map of cellular states and transitions and ultimately offering insights into how to control these processes. Furthermore, integrating this protocol into 3D retinal organoid models could enable more complex tissue architecture and intercellular interactions, better simulating the in vivo environment.

This work has attempted to present a comprehensive analysis of a 2D protocol for differentiating hIPSCs into PhR-like cells, demonstrating its reproducibility, flexibility, and potential for downstream applications. The findings lay a foundation for future research aimed at advancing our understanding of PhR biology and developing effective treatments for retinal degenerative diseases.

APPENDIX 1. SUPPLEMENTARY TABLE 1. PRIMARY AND SECONDARY DIFFERENTIATION MEDIUM

To access the data, click or select the words "Appendix 1."

APPENDIX 2. SUPPLEMENTARY TABLE 2. PRIMARY AND SECONDARY DIFFERENTIATION MEDIUM

To access the data, click or select the words "Appendix 2."

APPENDIX 3. SUPPLEMENTARY TABLE 3. PRIMARY AND SECONDARY ANTIBODIES

To access the data, click or select the words "Appendix 3."

APPENDIX 4. SUPPLEMENTARY TABLE 4. PRIMARY AND SECONDARY ANTIBODIES

To access the data, click or select the words "Appendix 4."

APPENDIX 5. SUPPLEMENTARY FIGURE 1. FLOW CYTOMETRIC ANALYSIS OF 661W CELLS AND PGP1-HIPSC-DERIVED CELLS AT DAY 52 OF DIFFERENTIATION (EXPERIMENT 2).

To access the data, click or select the words "Appendix 5." Both cell populations were fixed and stained with the photoreceptor marker RCVRN and/or a secondary antibody-only control. The analysis demonstrates marker-specific fluorescence, enabling comparison of photoreceptor marker expression between the established 661W cell line and hIPSC-derived cells.

APPENDIX 6. SUPPLEMENTARY FIGURE 2. FLOW CYTOMETRIC ANALYSIS OF PGP1-HIPSC-DERIVED CELLS AT DAY 42 OF DIFFERENTIATION (EXPERIMENT 3) AND 661W CONTROL CELLS.

To access the data, click or select the words "Appendix 6." Cells were stained with photoreceptor markers RCVRN, OPSN-S and OPSN-ML. 661W cells served as positive control.

APPENDIX 7. SUPPLEMENTARY FIGURE 3. FLOW CYTOMETRIC COMPARISON OF FIXED AND LIVE PGP1-HIPSC-DERIVED CELLS AT DAY 49 OF DIFFERENTIATION (EXPERIMENT 3) WITH 661W CONTROL CELLS.

To access the data, click or select the words "Appendix 7." Cells were stained with the photoreceptor marker RCVRN. Both fixed and live populations of PGP1-derived cells were analyzed, with 661W cells serving as controls.

APPENDIX 8. SUPPLEMENTARY TABLE 5. PRIMERS FOR RT-QPCR

To access the data, click or select the words "Appendix 8."

APPENDIX 9. SUPPLEMENTARY FIGURE 4. GENE EXPRESSION DYNAMICS ACROSS FIVE DIFFERENTIATION TIMEPOINTS IN PGP1-IPSC-DERIVED PHOTORECEPTORS.

To access the data, click or select the words "Appendix 9." Expression profiles of key genes were assessed at days 0, 6, 30, 40, and 59 during the photoreceptor (PhR) differentiation protocol in Experiment 2 (orange) and Experiment 3 (green). Data are presented as fold-change values normalized

to the reference gene GAPDH and scaled to the maximum expression level for each gene. The graphs illustrate temporal expression patterns, including early expression of the pluripotency marker OCT4, followed by the eye-field marker OTX2, activation of the neural retinal progenitor marker VSX2, and early photoreceptor lineage markers PRDM1, CRX, RCVRN and NR2F2. Quantitative PCR analysis across differentiation timepoints revealed distinct temporal patterns in gene expression associated with the transition from pluripotent hIPSCs to photoreceptor (PhR) progenitors. Expression of the pluripotency marker OCT4 declined sharply by day 9 (D9), confirming early exit from the pluripotent state. The retinal specification marker OTX2 peaked at D9 before gradually decreasing, with experiment-specific variation in the rate of decline. VSX2, a marker of retinal progenitor cells, showed temporally distinct expression profiles between experiments, suggesting differences in progenitor proliferation dynamics. PRDM1, associated with PhR lineage commitment, exhibited variable expression patterns, indicating experiment-dependent timing of PhR progenitor emergence. The photoreceptor transcription factor CRX displayed fluctuating expression peaks and declines, reflecting variability in post-mitotic PhR specification. Photoreceptor markers NR2F2 and RCVRN consistently peaked at D30, followed by a tapering phase. These findings underscore key regulatory windows and inter-experimental variability in PhR differentiation trajectories.

APPENDIX 10. SUPPLEMENTARY FIGURE 5. CONTROL STAINING FOR PROTEIN EXPRESSION IN 661W AND PGP1-HIPSC CELL LINES.

To access the data, click or select the words "Appendix 10." **A.** Immunocytochemical analysis of the 661W photoreceptor cell line showing expression of key photoreceptor and structural proteins: CX36, TMEM138, OPSN-M/L, CRX, ARR, OPSN-S, RCVRN, Phalloidin (PHAL) and NR2F2. **B.** Control staining of the human PGP1-IPSC line demonstrating expression of human mitochondrial marker, hMITO. **C.** Secondary antibody-only controls used throughout the study to validate specificity of primary antibody staining. Hoechst 33342 was used to label cell nuclei in all panels.

APPENDIX 11. SUPPLEMENTARY TABLE 6. CHARACTERISATION ASSAY

To access the data, click or select the words "Appendix 11."

APPENDIX 12. SUPPLEMENTARY TABLE 7. CHARACTERISATION ASSAY

To access the data, click or select the words "Appendix 12."

APPENDIX 13. SUPPLEMENTARY TABLE 8. CHARACTERISATION ASSAY

To access the data, click or select the words "Appendix 13."

APPENDIX 14. SUPPLEMENTARY FIGURE 6. LIVE MCHERRY FLUORESCENCE IN PGP1-REPORTER CELLS DURING PHOTORECEPTOR DIFFERENTIATION ACROSS THREE INDEPENDENT EXPERIMENTS.

To access the data, click or select the words "Appendix 14." Representative images showing live mCherry fluorescence at comparable timepoints during the differentiation protocol in Experiments 1, 2, and 3. Fluorescence reflects activation of the photoreceptor-specific reporter, indicating progression toward the photoreceptor lineage.

APPENDIX 15. SUPPLEMENTARY FIGURE 7. ULTRASTRUCTURAL ANALYSIS OF HIPSC-DERIVED PHOTORECEPTORS (PHRS) AND COMPARISON WITH 661W CELLS.

To access the data, click or select the words "Appendix 15." **A**. Representative image of hIPSC-derived PhRs at D50 of differentiation in Exp 3. Scale bar: 20 µm. **B**. Magnified and annotated view of panel A, showing cells in a linear arrangement with distinguishable nuclei (Nu), inner segments (IS), mitochondria (m), calyceal processes, defined Golgi apparatus, telodendria, and putative opsin-carrying vesicles (OCV). Scale bar: 10 µm. **C**. Image of hIPSC-derived PhRs at day 64 of differentiation in Exp 3, showing similar morphology to panel B, with abundant mitochondria (m) and visible nuclei (Nu). **D.** Representative image of 661W photoreceptor-like cells used for morphological comparison.

ACKNOWLDEGMENTS

This study was supported by funding provided by the Clem Jones Foundation (Brisbane, QLD, Australia) and the Cutmore Bequest provided to Bond University, Gold Coast, QLD, Australia. Conflict of Interest: The authors have no relevant financial or non-financial interests to declare that are relevant to the content of this article.

REFERENCES

1. Vyawahare H, Shinde P. Age-Related Macular Degeneration: Epidemiology, Pathophysiology, Diagnosis, and Treatment. Cureus 2022; 14:e29583[PMID: 36312607].

2. Cross N, van Steen C, Zegaoui Y, Satherley A, Angelillo L. Retinitis Pigmentosa: Burden of Disease and Current Unmet

Needs. Clin Ophthalmol 2022; 16:1993-2010. [PMID: 35757022].

3. Mitchell P, Liew G, Gopinath B, Wong TY. Age-related macular degeneration. Lancet 2018; 392:1147-59. [PMID: 30303083].

4. Shin JY, Ma D, Lim MS, Cho MS, Kim YJ, Yu HG. Embryonic stem cell-derived photoreceptor precursor cells differentiated by coculture with RPE cells. Mol Vis 2021; 27:288-99. [PMID: 34012231].

5. Pfau M, von der Emde L, de Sisternes L, Hallak JA, Leng T, Schmitz-Valckenberg S, Holz FG, Fleckenstein M, Rubin DL. Progression of Photoreceptor Degeneration in Geographic Atrophy Secondary to Age-related Macular Degeneration. JAMA Ophthalmol 2020; 138:1026-34. [PMID: 32789526].

6. Hushmandi K, Lam HY, Wong WM, Tan W, Daryabari SH, Reiter RJ, Farahani N, Kumar AP. Gene therapy for age-related macular degeneration: a promising frontier in vision preservation. Cell Commun Signal 2025; 23:233-[PMID: 40394614].

7. Ribeiro J, Procyk CA, West EL, O'Hara-Wright M, Martins MF, Khorasani MM, Hare A, Basche M, Fernando M, Goh D, Jumbo N, Rizzi M, Powell K, Tariq M, Michaelides M, Bainbridge JWB, Smith AJ, Pearson RA, Gonzalez-Cordero A, Ali RR. Restoration of visual function in advanced disease after transplantation of purified human pluripotent stem cell-derived cone photoreceptors. Cell Rep 2021; 35:109022[PMID: 33882303].

8. Politi LE, Lehar M, Adler R. Development of neonatal mouse retinal neurons and photoreceptors in low density cell culture. Invest Ophthalmol Vis Sci 1988; 29:534-43. [PMID: 3281914].

9. Lu AQ, Popova EY, Barnstable CJ. Activin Signals through SMAD2/3 to Increase Photoreceptor Precursor Yield during Embryonic Stem Cell Differentiation. Stem Cell Reports 2017; 9:838-52. [PMID: 28781074].

10. Garita-Hernandez M, Chaffiol A, Guibbal L, Routet F, Khabou H, Riancho L, Toualbi L, Picaud S, Sahel JA, Goureau O, Duebel J, Dalkara D. Control of Microbial Opsin Expression in Stem Cell Derived Cones for Improved Outcomes in Cell Therapy. Front Cell Neurosci 2021; 15:648210[PMID: 33815066].

11. Kelley RA, Chen HY, Swaroop A, Li T. Accelerated Development of Rod Photoreceptors in Retinal Organoids Derived from Human Pluripotent Stem Cells by Supplementation with 9-*cis* Retinal. STAR Protoc 2020; 1:100033[PMID: 32728670].

12. Saha A, Capowski E, Fernandez Zepeda MA, Nelson EC, Gamm DM, Sinha R. Cone photoreceptors in human stem cell-derived retinal organoids demonstrate intrinsic light responses that mimic those of primate fovea. Cell Stem Cell 2022; 29:460-471.e3. [PMID: 35104442].

13. Kallman A, Capowski EE, Wang J, Kaushik AM, Jansen AD, Edwards KL, Chen L, Berlinicke CA, Joseph Phillips M, Pierce EA, Qian J, Wang TH, Gamm DM, Zack DJ. Investigating cone photoreceptor development using patient-derived NRL null retinal organoids. Commun Biol 2020; 3:82-[PMID: 32081919].

14. Beaver D, Limnios IJ. A treatment within sight: challenges in the development of stem cell-derived photoreceptor therapies for retinal degenerative diseases. Front Transplant 2023; 2:1130086[PMID: 38993872].

15. Forrest D, Swaroop A. Minireview: the role of nuclear receptors in photoreceptor differentiation and disease. Mol Endocrinol 2012; 26:905-15. [PMID: 22556342].

16. Kaewkhaw R, Kaya KD, Brooks M, Homma K, Zou J, Chaitankar V, Rao M, Swaroop A. Transcriptome Dynamics of Developing Photoreceptors in Three-Dimensional Retina Cultures Recapitulates Temporal Sequence of Human Cone and Rod Differentiation Revealing Cell Surface Markers and Gene Networks. Stem Cells 2015; 33:3504-18. [PMID: 26235913].

17. Zheng Y, Chen S. Transcriptional precision in photoreceptor development and diseases - Lessons from 25 years of CRX research. Front Cell Neurosci 2024; 18:1347436[PMID: 38414750].

18. Swaroop A, Kim D, Forrest D. Transcriptional regulation of photoreceptor development and homeostasis in the mammalian retina. Nat Rev Neurosci 2010; 11:563-76. [PMID: 20648062].

19. Lam PT, Gutierrez C, Rio-Tsonis KD, Robinson ML. Generation of a Retina Reporter hiPSC Line to Label Progenitor, Ganglion, and Photoreceptor Cell Types. Bioarch. 2019;658963.

20. Foltz LP, Clegg DO. Rapid, Directed Differentiation of Retinal Pigment Epithelial Cells from Human Embryonic or Induced Pluripotent Stem Cells. J Vis Exp 2017; 12856274-[PMID: 29155780].

21. Limnios IJ, Chau YQ, Skabo SJ, Surrao DC, O'Neill HC. Efficient differentiation of human embryonic stem cells to retinal pigment epithelium under defined conditions. Stem Cell Res Ther 2021; 12:248-[PMID: 33883023].

22. Beers J, Gulbranson DR, George N, Siniscalchi LI, Jones J, Thomson JA, Chen G. Passaging and colony expansion of human pluripotent stem cells by enzyme-free dissociation in chemically defined culture conditions. Nat Protoc 2012; 7:2029-40. [PMID: 23099485].

23. Wheway G, Nazlamova L, Turner D, Cross S. 661W Photoreceptor Cell Line as a Cell Model for Studying Retinal Ciliopathies. Front Genet 2019; 10:308-[PMID: 31024622].

24. Al-Ubaidi MR, Matsumoto H, Kurono S, Singh A. Proteomics profiling of the cone photoreceptor cell line, 661W. Adv Exp Med Biol 2008; 613:301-11. [PMID: 18188958].

25. Kozera B, Rapacz M. Reference genes in real-time PCR. J Appl Genet 2013; 54:391-406. [PMID: 24078518].

26. Lam PT, Gutierrez C, Del Rio-Tsonis K, Robinson ML. Generation of a Retina Reporter hiPSC Line to Label Progenitor, Ganglion, and Photoreceptor Cell Types. Transl Vis Sci Technol 2020; 9:21-[PMID: 32714647].

27. Chew SH, Martinez C, Chirco KR, Kandoi S, Lamba DA. Timed Notch Inhibition Drives Photoreceptor Fate Specification in Human Retinal Organoids. Invest Ophthalmol Vis Sci 2022; 63:12-[PMID: 36129723].

28. Ripps H, Shen W. Review: taurine: a "very essential" amino acid. Mol Vis 2012; 18:2673-86. [PMID: 23170060].

29. Gaucher D, Arnault E, Husson Z, Froger N, Dubus E, Gondouin P, Dherbécourt D, Degardin J, Simonutti M, Fouquet S, Benahmed MA, Elbayed K, Namer IJ, Massin P, Sahel JA, Picaud S. Taurine deficiency damages retinal neurones: cone photoreceptors and retinal ganglion cells. Amino Acids 2012; 43:1979-93. [PMID: 22476345].

30. Shivaraj MC, Marcy G, Low G, Ryu JR, Zhao X, Rosales FJ, Goh ELK. Taurine induces proliferation of neural stem cells and synapse development in the developing mouse brain. PLoS One 2012; 7:e42935[PMID: 22916184].

31. Young TL, Matsuda T, Cepko CL. The noncoding RNA taurine upregulated gene 1 is required for differentiation of the murine retina. Curr Biol 2005; 15:501-12. [PMID: 15797018].

32. Eldred KC, Hadyniak SE, Hussey KA, Brenerman B, Zhang PW, Chamling X, Sluch VM, Welsbie DS, Hattar S, Taylor J, Wahlin K, Zack DJ, Johnston RJ Jr. Thyroid hormone signaling specifies cone subtypes in human retinal organoids. Science 2018; 362:eaau6348[PMID: 30309916].

33. McNerney C, Johnston RJ Jr. Thyroid hormone signaling specifies cone photoreceptor subtypes during eye development: Insights from model organisms and human stem cell-derived retinal organoids. Vitam Horm 2021; 116:51-90. [PMID: 33752828].

34. Kim JW, Yang HJ, Brooks MJ, Zelinger L, Karakülah G, Gotoh N, Boleda A, Gieser L, Giuste F, Whitaker DT, Walton A, Villasmil R, Barb JJ, Munson PJ, Kaya KD, Chaitankar V, Cogliati T, Swaroop A. NRL-Regulated Transcriptome Dynamics of Developing Rod Photoreceptors. Cell Rep 2016; 17:2460-73. [PMID: 27880916].

35. Ghinia Tegla MG, Buenaventura DF, Kim DY, Thakurdin C, Gonzalez KC, Emerson MM. OTX2 represses sister cell fate choices in the developing retina to promote photoreceptor specification. Elife 2020; 9:e54279[PMID: 32347797].

36. Zhang S, Cui W. Sox2, a key factor in the regulation of pluripotency and neural differentiation. World J Stem Cells 2014; 6:305-11. [PMID: 25126380].

37. Kondoh H, Uchikawa M, Ishii Y. Chapter 7 - Regulation of Sox2 via Many Enhancers of Distinct Specificities. Academic Press. 2016;217–33.

38. Roberts MR, Hendrickson A, McGuire CR, Reh TA. Retinoid X receptor (γ) is necessary to establish the S-opsin gradient in cone photoreceptors of the developing mouse retina. Invest Ophthalmol Vis Sci 2005; 46:2897-904. [PMID: 16043864].

39. Tan E, Ding XQ, Saadi A, Agarwal N, Naash MI, Al-Ubaidi MR. Expression of cone-photoreceptor-specific antigens in a cell line derived from retinal tumors in transgenic mice. Invest Ophthalmol Vis Sci 2004; 45:764-8. [PMID: 14985288].

40. Brunet AA, James RE, Swanson P, Carvalho LS. A review of the 661W cell line as a tool to facilitate treatment development for retinal diseases. Cell Biosci 2025; 15:41-[PMID: 40170180].

41. Roque RS, Rosales AA, Jingjing L, Agarwal N, Al-Ubaidi MR. Retina-derived microglial cells induce photoreceptor cell death in vitro. Brain Res 1999; 836:110-9. [PMID: 10415410].

42. Agarwal D, Kuhns R, Dimitriou CN, Barlow E, Wahlin KJ, Enke RA. Bulk RNA sequencing analysis of developing human induced pluripotent cell-derived retinal organoids. Sci Data 2022; 9:759-[PMID: 36494376].

43. Hussey KA, Hadyniak SE, Johnston RJ Jr. Patterning and Development of Photoreceptors in the Human Retina. Front Cell Dev Biol 2022; 10:878350[PMID: 35493094].

44. Gonzalez-Cordero A, Kruczek K, Naeem A, Fernando M, Kloc M, Ribeiro J, Goh D, Duran Y, Blackford SJI, Abelleira-Hervas L, Sampson RD, Shum IO, Branch MJ, Gardner PJ, Sowden JC, Bainbridge JWB, Smith AJ, West EL, Pearson RA, Ali RR. Recapitulation of Human Retinal Development from Human Pluripotent Stem Cells Generates Transplantable Populations of Cone Photoreceptors. Stem Cell Reports 2017; 9:820-37. [PMID: 28844659].

45. Collin J, Mellough CB, Dorgau B, Przyborski S, Moreno-Gimeno I, Lako M. Using Zinc Finger Nuclease Technology to Generate CRX-Reporter Human Embryonic Stem Cells as a Tool to Identify and Study the Emergence of Photoreceptors Precursors During Pluripotent Stem Cell Differentiation. Stem Cells 2016; 34:311-21. [PMID: 26608863].

46. Wu Y, Qiu J, Chen S, Chen X, Zhang J, Zhuang J, Liu S, Yang M, Zhou P, Chen H, Ge J, Yu K, Zhuang J. Crx Is Posttranscriptionally Regulated by Light Stimulation in Postnatal Rat Retina. Front Cell Dev Biol 2020; 8:174-[PMID: 32318566].

47. . HAIDER NB. DEMARCO P, NYSTUEN AM, HUANG X, SMITH RS, MCCALL MA, NAGGERT JK, NISHINA PM. The transcription factor Nr2e3 functions in retinal progenitors to suppress cone cell generation. Vis Neurosci 2006; 23:917-29. .

48. Aísa-Marín I, Rovira Q, Díaz N, Calvo-López L, Vaquerizas JM, Marfany G. Specific photoreceptor cell fate pathways are differentially altered in NR2E3-associated diseases. Neurobiol Dis 2024; 194:106463[PMID: 38485095].

49. Goodson NB, Kaufman MA, Park KU, Brzezinski JA 4th. Simultaneous deletion of *Prdm1* and *Vsx2* enhancers in the retina alters photoreceptor and bipolar cell fate specification, yet differs from deleting both genes. Development 2020; 147:dev190272[PMID: 32541005].

50. Brzezinski JA 4th, Lamba DA, Reh TA. Blimp1 controls photoreceptor versus bipolar cell fate choice during retinal development. Development 2010; 137:619-29. [PMID: 20110327].

51. Katoh K, Omori Y, Onishi A, Sato S, Kondo M, Furukawa T. Blimp1 suppresses Chx10 expression in differentiating

retinal photoreceptor precursors to ensure proper photoreceptor development. J Neurosci 2010; 30:6515-26. [PMID: 20463215].

52. Brzezinski JA 4th, Uoon Park K, Reh TA. Blimp1 (Prdm1) prevents re-specification of photoreceptors into retinal bipolar cells by restricting competence. Dev Biol 2013; 384:194-204. [PMID: 24125957].

53. Lamba DA, McUsic A, Hirata RK, Wang PR, Russell D, Reh TA. Generation, purification and transplantation of photoreceptors derived from human induced pluripotent stem cells. PLoS One 2010; 5:e8763[PMID: 20098701].

54. Cornish EE, Xiao M, Yang Z, Provis JM, Hendrickson AE. The role of opsin expression and apoptosis in determination of cone types in human retina. Exp Eye Res 2004; 78:1143-54. [PMID: 15109921].

55. Afanasyeva TAV, Corral-Serrano JC, Garanto A, Roepman R, Cheetham ME, Collin RWJ. A look into retinal organoids: methods, analytical techniques, and applications. Cell Mol Life Sci 2021; 78:6505-32. [PMID: 34420069].

56. Spirig SE, Renner M. Toward Retinal Organoids in High-Throughput. Cold Spring Harb Perspect Med 2024; 14:a041275[PMID: 37217280].

57. Rashidi H, Leong YC, Venner K, Pramod H, Fei QZ, Jones OJR, Moulding D, Sowden JC. Generation of 3D retinal tissue from human pluripotent stem cells using a directed small molecule-based serum-free microwell platform. Sci Rep 2022; 12:6646-[PMID: 35459774].